Polymers of Intrinsic Microporosity Containing Troger Base for CO2 Capture

I&EC research
Industrial & Engineering Chemistry Research

ACS AuthorChoice

Article

pubs.acs.org/IECR

Polymers of Intrinsic Microporosity Containing Tröger Base for CO_2 Capture

Annalaura Del Regno,[†,¶] Aleksandra Gonciaruk,[†,¶] Laura Leay,[†] Mariolino Carta,[‡] Matthew Croad,[‡] Richard Malpass-Evans,[‡] Neil B. McKeown,[‡] and Flor R. Siperstein*[,†]

[†]School of Chemical Engineering and Analytical Science, The University of Manchester, Manchester M13 9PL, United Kingdom
[‡]School of Chemistry, Cardiff University, Cardiff CF10 3AT, United Kingdom

Supporting Information

ABSTRACT: Properties of four polymers of intrinsic microporosity containing Tröger's base units were assessed for CO_2 capture experimentally and computationally. Structural properties included average pore size, pore size distribution, surface area, and accessible pore volume, whereas thermodynamic properties focused on density, CO_2 sorption isotherms, and enthalpies of adsorption. It was found that the shape of the contortion site plays a more important role than the polymer density when assessing the capacity of the material, and that the presence of a Tröger base unit only slightly affects the amount adsorbed at low pressures, but it does not have any significant influence on the enthalpy of adsorption fingerprint. A comparison of the materials studied with those reported in the literature allowed us to propose a set of guidelines for the design of polymers for CO_2 capture applications.

INTRODUCTION

The potential of polymeric membranes in gas separation applications has been known for over 150 years.[1] The first commercially available membrane dates back to the 1970s when Permea introduced the first hydrogen-separating membrane (Prism membrane),[2,3] lately commercialized in 1979 by Mosanto,[4] and during the mid-1980s, Generon introduced a membrane (TPX) for nitrogen−air separation.[5] Since then, membranes for gas separations are considered a proven technology widely used in industry and studied in academia; according to Baker, 90% of installed gas separation membrane units use polymeric membrane as part of their processes.[5,6] Polymers offer a wide range of advantages for gas separations: their chemistry can be tailored to achieve desired selectivity and because of the ease of polymer processability and flexibility, light and very thin membranes can be created. However, the most selective polymers, such as polyimides, polysulfones, and polycarbonates, have a relatively low free volume, which results in low gas permeability; for this reason, only a few polymers have gained commercial success,[7−9] but research in the development of high-free volume polymers is increasing.

In 1983, Masuda et al.[10] introduced the polyacetylene poly[1-(trimethylsilyl)-1-propyne] (PTMSP), which had the highest O_2 permeability among all polymers known at that time; PTMSP is still used as a reference for newly synthesized high free volume polymers. The extremely high permeability in PTMSP is the result of the rigid and bulky structure that prevents it from filling space efficiently, thus creating intermolecular free volume. During the past decade, a series of new microporous polymers has been introduced, where rigidity and contortion play a major role in the microporosity of the resulting materials.[11−19]

First introduced in 2004 by Budd et al.,[11] polymers of intrinsic microporosity (PIMs) are an emerging class of amorphous glassy polymers which appear promising for efficient gas separations. They present a series of appealing characteristics for gas separation such as high micropore volume, tunable chemistry, relatively noncomplex and versatile processability, stability, and synthetic reproducibility.[20]

Microporosity in PIMs is achieved by reducing rotational freedom within the polymer chain by inserting contortion sites, thus increasing accessible surface area for adsorptive molecules. The surface area of PIMs ranges from 300 to 1760 $m^2\ g^{-1}$.[15] There are a variety of monomers (Figure 1) that can be used to synthesize PIMs; the contorted structure can be imposed by either using a spirocenter (Figure 1a and b) or steric crowding around the covalent bond (Figure 1c); a comprehensive

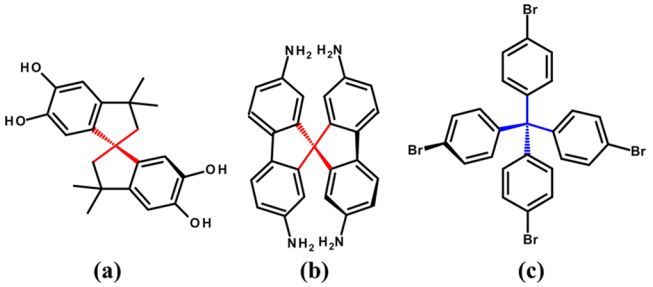

Figure 1. An example of possible monomers for PIM synthesis. The spirocenters are shown in red (a and b), and restricted motion about the central carbon due to steric crowding is shown in blue (c). Monomer a is commonly used in linear polymers and monomers b and c lead to network polymers.

Received: August 29, 2013
Revised: November 1, 2013
Accepted: November 1, 2013
Published: November 1, 2013

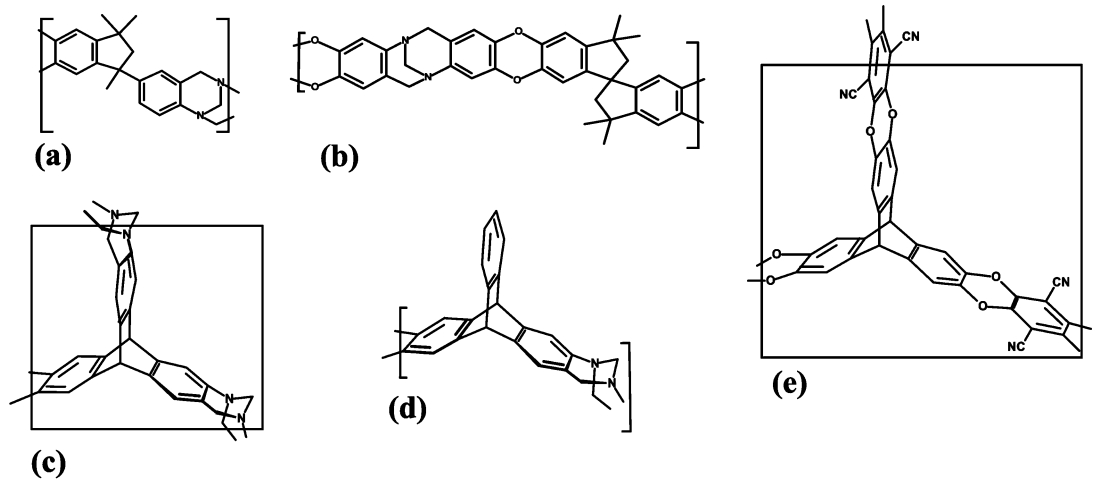

Figure 2. Chemical structure of the PIMs investigated in this study. (a) PIM-Indan-TB, (b) PIM-TB-cat-A, (c) PIM-Trip-TB network, (d) PIM-Trip-TB ladder, and (e) Trip(H)-PIM.

collection of contortion and steric crowding sites are reported in the literature.[15,20] Hence, the desired properties of PIMs can be tailored by introducing a suitable comonomer or functional group into the polymer chain, thereby enhancing the performance of the sorbent (e.g., selectivity, capacity, or solubility).

The combination of microporosity and ability to generate solution-processable film-forming material offers unique benefits in membrane technology. PIMs-based membranes have been initially investigated in pervaporative separation of phenols from aqueous solutions,[11] showing high permeability as well as good separation factor and stability. For gas separation membranes,[21] data for PIMs demonstrate both high permeability and selectivity and, hence, crossed Robeson's upper bound[22] for several important gas pairs such as O_2/N_2 and CO_2/CH_4, which contributed to the revision of the upper bound in 2008.[23]

The empirical upper bound in the Robeson plot is used as an indicator of performance for novel materials. It is common for polymers possessing high selectivity to show low permeability and vice versa. One can surpass the bound by increasing permeability through enhanced backbone rigidity and contortion or increasing selectivity through incorporation of functional groups.[24]

Carta et al.[25] recently reported the synthesis of two Tröger's base (TB) PIMs, ethanoanthracene-based TB PIM (PIM-EA-TB) and spirobisindane-based TB PIM (PIM-SBI-TB). Although PIM-SBI-TB shows a lower surface area compared with that of PIM-1 as well as the usual permeability trend observed in PIMs (condensable gases are more permeable than smaller molecules, i.e., CO_2 and $CH_4 > H_2$), the addition of an EA unit combined with TB lead to a PIM, which has an increased surface area of 1028 $m^2\ g^{-1}$, and provided gas permeability data that surpassed the 2008 Robeson upper bound for O_2/N_2, H_2/N_2, H_2/CH_4, and H_2/CO_2 gas pairs. Although many PIMs can form films, some of them can only be obtained as powders (e.g., network PIMs), but due to their properties, potential use as adsorbents is an interesting alternative.

In this work, four novel Tröger's base polymers are investigated in CO_2 sorption. Two triptycene-based TB PIMs, spirobisindan- and indan-based TB PIMs have been studied and compared to Trip(H)-PIM network, known to be one of the most microporous amorphous networks prepared using the concept of intrinsic microporosity based on its high gas uptake.[26]

These materials were selected specifically to study the influence of structural and chemical properties of PIMs upon CO_2 sorption. In particular, the influence of the monomers' chemistry, overall structure, and rigidity of the contortion site were studied; by comparing the properties of Trip-PIM with those of Trip-TB network (both network polymers) and PIM-1 (vastly reported in literature) with TB-cat-A (all linear polymers), we can assess the effect of the TB site on network and linear PIMs; comparing the CO_2 adsorption capacity of Trip-TB network with that of Trip-TB ladder PIM allows assessment of the effect of networklike structures maintaining a specific contortion site, and we can determine the effect of a reduction in the rigidity of the contortion site by comparing the performances of TB-cat-A and Indan-TB. Experimentally measured isotherms are interpreted in terms of the dual-mode isotherm model to account for sorption and swelling of the sorbent, and a molecular-level description of the observed phenomena is discussed through molecular simulations to support experimental observation.

MATERIALS AND METHODS

Materials. In this work, four novel TB-containing PIMs have been tested as selective CO_2 sorbents and compared with the previously reported Trip(H)-PIM network (Figure 2).[26]

The TB-containing polymers PIM-Indan-TB, PIM-TB-cat-A, network-PIM-Trip-TB, and ladder-PIM-Trip-TB were prepared from the TB-forming polymerization reaction of the respective diamine or triamine monomers with dimethoxymethane in trifluoroacetic acid, as will be described fully elsewhere;[27] similar materials have been recently reported by Zhu et al.[28] The 1,1,3-trimethyl-3-phenyl unit of PIM-Indan-TB is relatively flexible and possesses a single covalent C−C bond around which conformational rotation may take place. In contrast, the bridged bicyclic triptycene and TB units are conformationally locked and rigid.

Experimental Method. CO_2 sorption isotherms of the polymers were collected by static gravimetric technique using a Hiden Isochema's Intelligent Gravimetric Analyzer (IGA-001). The samples were pretreated to ensure complete contaminant evacuation; the pretreatment consisted of a thermal degassing

dx.doi.org/10.1021/ie402846a | Ind. Eng. Chem. Res. 2013, 52, 16939−16950

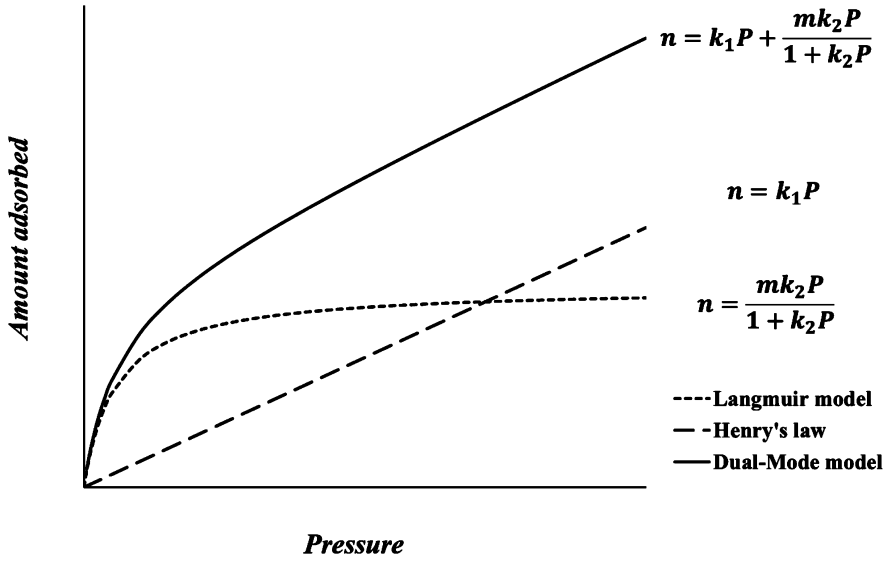

Figure 3. Representation of the dual mode sorption model and contribution of Langmuir and Henry's isotherm models.

at 373 K for 3 h, followed by a slow increase of temperature at the rate of 2 K/min up to 473 K, and maintenance at 473 K for 8 h under vacuum using a turbomolecular pump. Helium isotherms were measured at 293 K at the end of the pretreatment to asses the buoyancy effect and to determine the density of the polymers. The assumption in the determination of the density is that helium does not adsorb, and the apparent change of weight with pressure is due to the sample buoyancy. A force balance in the system taking into consideration all components of the balance, allows calculating the sample density. CO_2 isotherms were measured between vacuum and 20 bar pressure at constant temperature (293 and 333 K). The initial pressure intervals (vacuum to 1 bar) were set at 0, 0.1, 0.25, 0.5, 0.75, and 1 bar in order to obtain better representation at low pressures where rapid CO_2 uptake was expected. The pressure was then increased in 1 bar increments until the final 20 bar pressure was reached. The system was allowed to equilibrate at each pressure for a maximum of three hours; therefore, some of the values reported in the isotherms corresponds to pseudoequilibrium points.

Surface area was measured by nitrogen adsorption at 77 K using an automated BET analyzer (Micromeritics TriStar). Prior to testing, samples were degassed at 503 K under flowing nitrogen for 8 h in a sample degas system (Micromeritics FlowPrep 060). Surface areas were calculated within a range of relative pressure between 0.06 and 0.32 P/P_0.

Dual Mode Sorption. Collected isotherms were described by the dual mode sorption (DM) model. The DM model is conventionally used to represent sorption of gases in glassy polymers. This concept was first suggested by Meares in 1954[29] and further developed by Barrer et al., Michaels et al., and Vieth et al.[30−32]

The theory recognizes two sorption mechanisms present in glassy polymers.[1] One population of gas molecules dissolves in the polymer matrix following the Henry's law, a mechanism commonly observed in rubbery polymers, and molecules filling the microcavities behave according to the Langmuir model, that is, the sorbate molecules rapidly fill unrelaxed free volume of the glassy polymer at lower pressures, whereas at higher pressures, saturation capacity of the adsorbent is reached.

The DM isotherm is typically expressed as

$$n = n_1 + n_2 = k_1P + \frac{mk_2P}{1 + k_2P} \quad (1)$$

where n_1 and n_2 represents the amount adsorbed (mmol g^{-1}) based on Henry's law and the Langmuir model, respectively, k_1 is Henry's law dissolution constant (mmol g^{-1} bar^{-1}) representing affinity between bulk polymer and adsorbate, P is the pressure (bar), m is the Langmuir saturation capacity constant (mmol g^{-1}), and k_2 is the Langmuir pore affinity constant (bar^{-1}). Figure 3 shows a graphic representation of the DM model and the Langmuir and Henry's law models' contributions. To assess goodness of fit, the mean relative percent deviation modulus, E (%), was calculated, defined by

$$E = \frac{1}{N}\sum_{i=1}^{n}\left|\frac{m_i - m_{pi}}{m_i}\right| \times 100\% \quad (2)$$

where m_i is the experimental value, m_{pi} is the predicted value by the model, N is the number of experimental data points. The modulus value below 10% indicates an acceptable fit for practical use.[33]

Enthalpy of Adsorption. Isotherms described by the DM model were used to calculate the enthalpies of adsorption, ΔH, from the equation

$$\ln\frac{P_2}{P_1} = \frac{\Delta H}{R}\left(\frac{1}{T_1} - \frac{1}{T_2}\right) \quad (3)$$

where P_1 and P_2 are the pressures at the temperatures T_1 and T_2, respectively, and calculated at the same value of n (amount of adsorbed gas) and R is the ideal gas constant. Because the values of ΔH are very sensitive to the constants of mathematical models that are used for their estimation, it is important not to extrapolate. Therefore, only the range of concentrations that was valid for isotherms at both temperatures was used.

Solubility. For every species studied, the total CO_2 solubility at infinite dilution (apparent Henry's law constant) was calculated. The solubility (S) of CO_2 in adsorbent can be expressed in terms of DM parameters:

dx.doi.org/10.1021/ie402846a | Ind. Eng. Chem. Res. 2013, 52, 16939−16950

$$S = \frac{n}{P} = k_1 + \frac{mk_2}{1 + k_2 P} \tag{4}$$

When pressure is extrapolated to zero, the denominator of eq 2 can be neglected, which yields total CO_2 solubility at infinite dilution

$$S_0 = \lim_{P \to 0} \left(k_1 + \frac{mk_2}{1 + k_2 P} \right) = k_1 + mk_2 \tag{5}$$

Computational Methods. *Polymers Structure.* Different approaches are reported in the literature to model polymers of intrinsic microporosity.[34−38] In this work, polymers were represented using fully atomistic models; the interaction between atoms were described using the Universal (Trip(H)-PIM)[39] and OPLS (TB-based polymers)[40] force fields; the charges were calculated for Trip(H)-PIM through the charge equilibration algorithm (QEq),[41] whereas for the TB-based polymers, the OPLS charges were used. The monomer units for the polymers studied were constructed using MOLDEN software.[42] Details of the virtual polymer preparation procedure used in this work are described in the Supporting Information. One set of the materials was prepared without solvent (Trip(H)-PIM, Trip-TB network, Trip-TB ladder, TB-cat-A, and Indan-TB), corresponding to an "aged" sample, and a second set was prepared with sufficient solvent molecules (Trip(H)-PIM-S, Trip-TB network-S, Trip-TB ladder-S, TB-cat-A-S, and Indan-TB-S) to match the experimentally measured density. The number of solvent molecules was adjusted to match the experimental density, and it is different in each polymer as reported in Table S1 of the Supporting Information. The solvent used in all cases was methanol because experimentally, it is the solvent used for the final washing of the polymer.[43]

Characterization of the Virtual Materials. Molecular models generated were characterized by their densities, surface areas, and pore size distribution. All results were averaged over three boxes generated from different initial configurations. The Poreblazer software[44] was used to calculate the porosity, surface area, and pore size distribution (PSD) of the simulated samples. The surface area is defined by rolling a probe molecule along the surface of atoms; a probe size equal to the diameter of a nitrogen molecule was used (d_{N_2} = 3.681 Å) as nitrogen was used to characterize surface area experimentally. The software uses a Monte Carlo (MC) procedure to assess pore size distribution. In the first MC round, the free space inside a simulation box is mapped dividing the cell by a grid and verifying which grid point (a) lies inside the free space (Figure 4); for every point that does not overlap with an atom of the structure, the distance between the point and the nearest atom's surface is found. In the second MC round, the largest sphere containing a random point a that does not overlap with the structure is found (Figure 4). At the end of the MC run, a fractional cumulative free volume $V_P(r)$ is determined; the PSD is defined as the derivative ($dV_P(r)/dr$). The PSD is calculated in $Å^{-1}$ units and can be converted into $cm^3\ g^{-1}\ Å^{-1}$ by normalizing the output by the polymer density for future comparison with experimental PSD. It is known that BET surface area may not correspond to the geometric surface area,[45−48] but we chose to characterize the materials using geometric surface area because it is not as computationally demanding as calculating N_2 adsorption isotherms at 77 K.

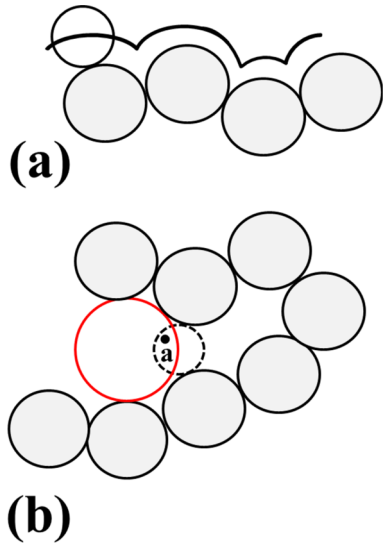

Figure 4. Schematic representation of (a) the accessible surface area and (b) the cumulative pore calculation. The red sphere represents the largest sphere containing the point *a*. Adapted from Sarkisov and Harrison.[44]

Grand Canonical Monte Carlo Simulation. GCMC simulations of carbon dioxide sorption at a fixed pressure of 0.05 bar and using the Henry's constant tool in the Sorption module in Materials Studio[49] were performed at 293.15 K.

Simulations were performed for samples generated without solvents and for samples matching the experimental density. Constraints were applied to prevent adsorption of CO_2 into inaccessible pores of the polymers' matrix. The parameters used to describe CO_2 are shown in Table 1. Intermolecular interactions were described by the Dreiding force field,[50] and the Lorentz−Berthelot mixing rules were used. The Lennard-Jones potential was used to estimate the van der Waals interactions; Coulombic interactions were calculated using the Ewald summation method. Charges for CO_2 and framework atoms were calculated using the Qeq method. A combination of translation, rotation, insertion, and deletion steps were performed for a total of 2×10^7 MC steps, including equilibration and collection points. For the Henry's constant simulations, 10×10^7 MC steps were used. All sorption data and Henry constants were modeled on the final configuration for each independent MD simulation, resulting in a total of three samples analyzed for each polymer. Results were averaged over three boxes for each generated system. Solubility was provided from the Henry's constant simulation, and enthalpy of adsorption was obtained from the fixed sorption GCMC simulations at a pressure of 0.05 bar.

Table 1. Lennard-Jones and Electrostatic Charges $q(e)$ for CO_2

CO_2			
atom type	$q(e)$	ε, K	σ, nm
C	+0.7510	47.86	0.3473
O	−0.3755	48.16	0.3033
d_{C-O} (nm)	0.1160		

dx.doi.org/10.1021/ie402846a | *Ind. Eng. Chem. Res.* 2013, 52, 16939−16950

Table 2. Experimental and Simulated Structural Properties of PIMs

	experimental data		simulated data[c]		simulated data[d]	
sorbent	density,[a] g cm^{-3}	ASA,[b] m^2 g^{-1}	density, g cm^{-3}	ASA, m^2 g^{-1}	density, g cm^{-3}	ASA, m^2 g^{-1}
Trip-TB ladder	0.903(11)	899(18)	1.253(18)	107(20)	0.905(9)	975(31)
Trip-TB network	0.937(10)	1035(25)	1.282(58)	96(68)	0.900(15)	918(67)
TB-cat-A	1.099(24)	525(10)	1.152(4)	199(46)	1.010(23)	350(99)
Indan-TB	0.894(5)	535(11)	1.131(10)	117(18)	0.918(16)	683(62)
Trip(H)-PIM	0.917(33)	1032(21)	1.213(4)	274(12)	0.916	1029

[a]Calculated through helium adsorption isotherms. [b]Calculated through BET measurements. [c]Sample generated without solvent. [d]Sample generated with solvent.

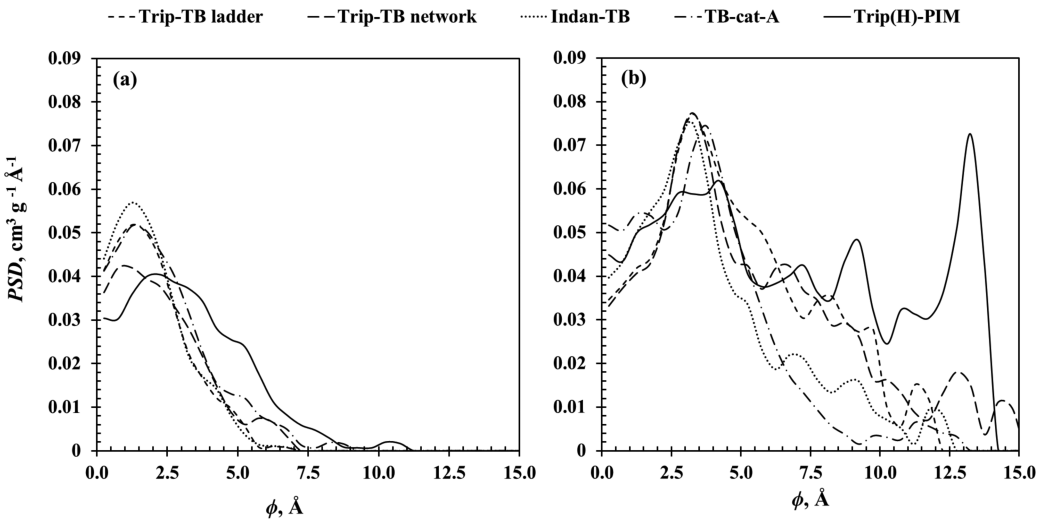

Figure 5. PSD of structure generated (a) without and (b) with solvent.

RESULTS AND DISCUSSION

Structural Properties. Experimental and simulated structural properties, such as density and accessible surface area (ASA) of the studied polymers are reported in Table 2.

Polymers containing the triptycene unit show the highest apparent BET surface area among the materials studied; as observed in previously synthesized triptycene based PIMs, the rigid monomer strongly influences the porosity of the systems. Experimentally, chain cross-linking results in higher surface area in the cases of Trip-TB network and Trip(H)-PIM compared to that of Trip-TB ladder. However, the simulated values of surface area in the case of Trip-TB network and ladder have the opposite trend to what is observed experimentally; the surface area of Trip-TB network is slightly lower than that of the ladder.

The error in density for Trip-TB network was 4 times higher than those for other polymers, and the error in surface area was approximately 3 times higher than those in the other materials simulated. Considering the fact that properties should converge if larger simulation boxes are used because a more representative description of the material is obtained, we would expect that more accurate results will be obtained using larger simulation boxes. The box sizes selected for this work are consistent with other studies reported in the literature for similar materials.[35,48,51−53] Therefore, it is surprising that Trip-TB network requires a larger box for convergence of the calculated properties. Nevertheless, a detailed analysis on the effect of box size on the properties of these polymers has not been made, and it is outside the scope of this work. Surface area of Trip(H)-PIM has a better agreement with the experimental value as the model consists of partially formed slabs that provide a better representation of the polymer's network.

TB-cat-A and Indan-TB both present lower surface area compared to that of their predecessor PIM-1, which has a surface area of 850 m^2 g^{-1}.[11]

In the case of TB-cat-A, the lower surface area can be explained by its higher density (1.099 versus the 0.94 g cm^{-3} reported by Larsen et al.[35]). In the Indan-TB case, the addition of extra flexibility created by a single bond in the spirocenter leads to a material that is packed more tightly. The higher density of TB-cat-A compared to that of Indan-TB can explain the difference in ASA observed in the simulated samples. The similarity in ASA measured experimentally for both samples is not captured by the model. It is possible that Indan-TB is more flexible than the chains modeled, creating a larger void volume of inaccessible pores. This observation is supported by the PSD of the simulated structure (Figure 5) for materials generated both with and without solvents; Indan-TB has the highest concentration of small pores inaccessible to nitrogen among the materials studied. This effect may be enhanced for more flexible chains.

Density is strongly overestimated and surface area is underestimated for modeled samples generated exclusively with polymer chains. It is well-known from literature that polymers with very high glass transition temperature (T_g) and very high free volume reach the T_g while still containing significant amount of solvents during solvent casting;[54] these polymers usually get locked in a very high nonequilibrium condition, yielding additional free volume that is created when the solvent is completely removed. Therefore, it is not surprising that models generated without solvent molecules

dx.doi.org/10.1021/ie402846a | Ind. Eng. Chem. Res. 2013, 52, 16939−16950

underestimate the surface area and overestimate the materials' density; they are representative of the aged polymers' properties. The aging process of PIMs,[43] PTMSP,[55,56] and glassy polymers in general has been reported in literature;[57,58] this effect can be reversed by treating the polymer with methanol and other compounds (ethanol, DMSO,DMAc, NMP, etc.).[43,54] Therefore, the addition of solvent molecules during the packing scheme was necessary to reproduce the properties of the polymers at nonequilibrium. Excellent agreement in surface area can be obtained with structures generated with the addition of solvents; this underlines the need to generate structures with sensible density, especially in cases where the modeled structure is used to predict properties of possible new monomer combinations.

The PSD curve for samples generated with and without solvent molecules show different trends of porosity, summarized in Tables 3 and 4. Differences in the PSD lead to different adsorption properties, which are discussed later.

Table 3. Free Volume versus Pore Size for Samples Generated without Solvent Molecules

	free volume per pore size, $cm^3\ g^{-1}$			
polymer	Φ < 3.3 Å	3.3 < Φ < 4.5 Å	Φ > 4.5 Å	total
Trip-TB ladder	0.067	0.011	0.003	0.082
Trip-TB network	0.059	0.014	0.007	0.080
TB-cat-A	0.070	0.015	0.011	0.097
Indan-TB	0.071	0.012	0.003	0.086
Trip(H)-PIM	0.057	0.023	0.023	0.103

Table 4. Free Volume versus Pore Size for Samples Generated with Solvent Molecules

	free volume per pore size, $cm^3\ g^{-1}$			
polymer	Φ < 3.3 Å	3.3 < Φ < 4.5 Å	Φ > 4.5 Å	total
Trip-TB ladder-S	0.078	0.050	0.109	0.237
Trip-TB network-S	0.077	0.046	0.118	0.241
TB-cat-A-S	0.084	0.050	0.051	0.184
Indan-TB-S	0.086	0.041	0.060	0.187
Trip(H)-PIM-S	0.080	0.044	0.185	0.310

The PSD for samples generated without obstacles shows the highest concentration of inaccessible pores to CO_2 (0.25−3.3 Å probe diameter) in the order of:

- Indan-TB > Trip-TB ladder > TB-cat-A > Trip-TB network > Trip(H)-PIM, whereas the concentration of small pores accessible to CO_2 (3.3−4.5 Å probe diameter) follows the trend Trip(H)-PIM > TB-cat-A > Trip-TB network > Trip-TB ladder ≥ Indan-TB.
- Trip(H)-PIM shows the highest concentration of large pores (4.5−11.0 Å probe diameter) among all the samples followed by TB-cat-A > Trip-TB network > Trip-TB ladder ≥ Indan-TB.

When obstacles are added to the simulation box to match the experimental density, the PSD trend changes.

- The distribution of inaccessible pores (0.25−3.3 Å probe diameter) follows the decreasing order of Indan-TB-S ≥ TB-cat-A-S > Trip-TB ladder-S ≥ Trip-TB network-S > Trip(H)-PIM-S, whereas the trend for accessible pores in the rage of 3.3−4.5 Å probe diameter is Trip-TB ladder-S ≥ TB-cat-A-S > Trip-TB network-S > Trip(H)-PIM-S > Indan-TB-S.
- Distribution of pores in the range of 4.5−15 Å probe diameter follows the order of Trip(H)-PIM-S > Trip-TB network-S > Trip-TB ladder-S > Indan-TB-S > TB-cat-A-S.
- The Dual Mode Sorption and Enthalpy of Adsorption sections show how the distribution of pore sizes affects the trend in CO_2 solubility and enthalpy of adsorption of the simulated polymers.

Sorption Isotherms. Experimentally measured CO_2 sorption isotherms on PIMs at two different temperatures are shown in Figure 6. Saturation capacity for all sorbents was not reached at any tested condition. Adsorption kinetics were slow and an increasing loading of CO_2 was observed at most isothermal points even after 3 h of equilibration (i.e., maximum time period to maintain constant pressure at the point); in such cases, no asymptote was reached; thus, the data reported in this work correspond to the pseudoequilibrium measurements.

The initially rapid uptake at lower pressures followed by a slower gain in loading at higher pressures was observed in all PIM samples. Such an adsorption pattern at lower pressures indicates microporosity of the samples and a process similar to

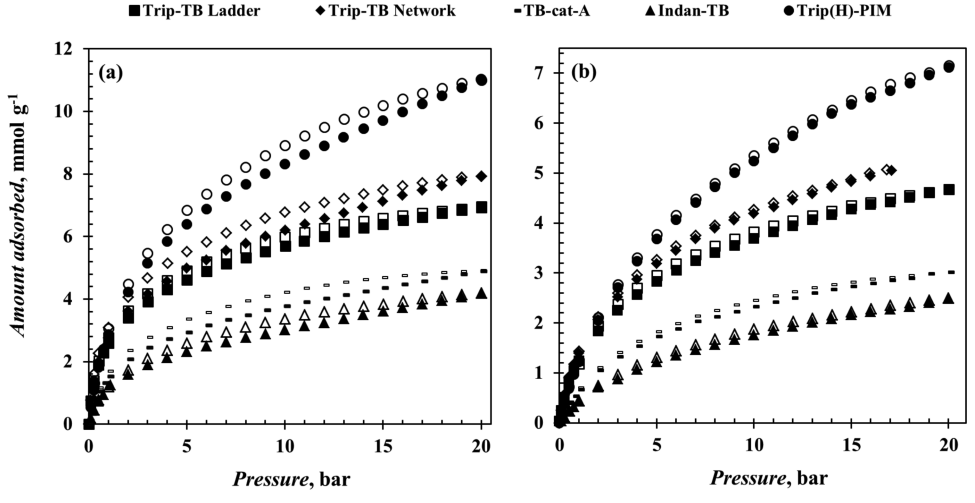

Figure 6. Experimental CO_2 sorption (filled symbols) and desorption (open symbols) isotherms at (a) 293 and (b) 333 K.

dx.doi.org/10.1021/ie402846a | Ind. Eng. Chem. Res. 2013, 52, 16939−16950

Table 5. Dual Mode Constants for Sorption of CO_2 for PIMs Studied in This Work

sorbent	density, g cm^{-3}	k_1, mmol g^{-1} bar^{-1}	m, mmol g^{-1}	k_2, bar^{-1}	T, K
Trip-TB ladder	0.903	0.183	3.812	2.028	293
		0.107	2.857	0.698	333
Trip-TB network	0.937	0.194	4.337	1.872	293
		0.133	3.059	0.773	333
TB-cat-A	1.099	0.130	2.568	1.339	293
		0.075	1.828	0.582	333
Indan-TB	0.894	0.121	1.933	1.105	293
		0.070	1.293	0.423	333
Trip(H)-PIM	0.917	0.263	6.309	0.813	293
		0.157	4.843	0.298	333

that observed in typical rigid microporous materials. At higher pressures (from about 10 to 20 bar), the amount of adsorbed CO_2 increased almost linearly, indicating that polymer swelling and relaxation became more significant, allowing further gas sorption into the polymer matrix. At both temperatures and in all PIMs, hysteresis was observed and the desorption isotherms were above the adsorption isotherms, closing the loop at low pressures (less than one bar). This can be explained by the polymer volume dilation and relaxation of chains, which proceeded even during desorption. The hysteresis loop was narrower at higher temperature and in linear polymers. At higher temperature, chains have higher kinetic energy, and linear polymers are not restricted by cross-linked bonds; thus, chains of molecules are more flexible and can return to their initial state more rapidly. The adsorptive capacity is an important parameter that has significant influence for the performance of the polymer. One of the main contributions to large CO_2 sorption capacities is high accessible surface area of the sorbent. Indeed, the highest CO_2 concentration among the polymers was measured for Trip(H)-PIM (11.02 mmol of CO_2 per g of sorbent at 20 bar and 293 K), which also possess the largest surface area.

The highest capacity recorded for Trip-TB Network, Trip-TB Ladder, TB-cat-A, and Indan-TB is 7.93, 6.96, 5.02, and 4.19 mmol g^{-1}, respectively, at 20 bar and 293 K and follows the decreasing trend of surface areas (Table 2).

Dual Mode Sorption. Experimental data of CO_2 sorption on PIMs were correlated using the previously discussed DM isotherm model. The constants for individual isotherms are available in the Supporting Information. The mean relative percentage deviation moduli were no greater than 4% in all cases; therefore, the DM model is considered adequate for describing CO_2 sorption on the PIM samples' data.

The average parameters in the DM model for the systems measured are presented in Table 5, and a comprehensive list of DM constants reported in the literature is available in the Supporting Information (Table S6).

The properties of the measured polymers can be arranged in descending order

- Henry's solubility (k_1): Trip(H)-PIM > Trip-TB Network > Trip-TB Ladder > TB-cat-A > Indan-TB.
- Langmuirian affinity (k_2): Trip-TB Ladder > Trip-TB Network > TB-cat-A > Indan-TB > Trip(H)-PIM.
- Langmuirian capacity (m): Trip(H)-PIM > Trip-TB Network > Trip-TB Ladder > TB-cat-A > Indan-TB.

Trip(H)-PIM has the highest Langmuirian capacity (m) as well as highest CO_2 solubility (k_1) among the samples measured in this work, and Indan-TB had the lowest k_1 and m values. In general, k_1 and m have the same trend as the CO_2 uptake in PIMs at higher pressures. At pressures below atmospheric, the adsorptive properties are predominantly defined by the surface chemistry of the adsorbent. Trip(H)-PIM adsorbs less CO_2 than Trip-TB network and Trip-TB ladder as shown in Figure 7. This is also reflected in the values of k_2, which indicates that PIMs containing TB have a higher affinity for CO_2 than Trip(H)-PIM.

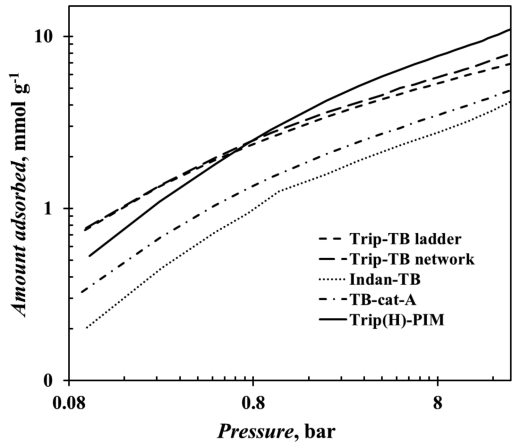

Figure 7. Log–log plot of isotherms of Trip-TB ladder, Trip-TB network, TB-cat-A, Indan-TB, and Trip(H)-PIM.

Extensive gas sorption data in glassy polymers (polycarbonates, polysulfones, polyimides, and polyarylates) described by the DM model have been reported in the literature.[59−69] DM constants and total solubility of some representative examples, reported in Supporting Information Table S6, have been used for comparison with the studied materials to asses the factors that contribute to enhanced CO_2 sorption. In Figures 8 and 9, total CO_2 solubility at infinite dilution and DM model constants as a function of polymer density of various glassy polymers are reported. Although the DM constants depend on various factors, such as glass transition temperature, fractional free volume, and measurement conditions,[70] independent of the polymer density and structure, it can be clearly seen that solubility and DM model constants of most polymers reported in the literature are very similar. Most data available in the literature is at 308 K. Even though our experiments were done at 293 and 333 K, it is possible to calculate the zero-coverage solubility at different temperatures using eqs 3−5. The open bars in Figure 8 show the calculated values at 303 K that can be directly compared to those in the literature.

dx.doi.org/10.1021/ie402846a | Ind. Eng. Chem. Res. 2013, 52, 16939−16950

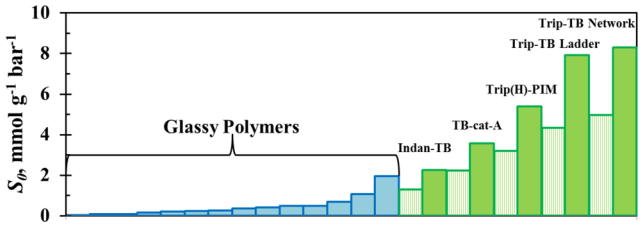

Figure 8. Total solubility at infinite dilution for Trip-TB Network, Trip-TB Ladder, Trip(H)-PIM, TB-cat-A, and Indan-TB. Solubilities calculated from experimental data at 293 K are represented by full green bars; calculated solubilities at 303 K are represented by open bars. For comparison, solubilities of other glassy polymers reported in literature[59−69,74] and in Table S6 (Supporting Information) are shown as blue bars.

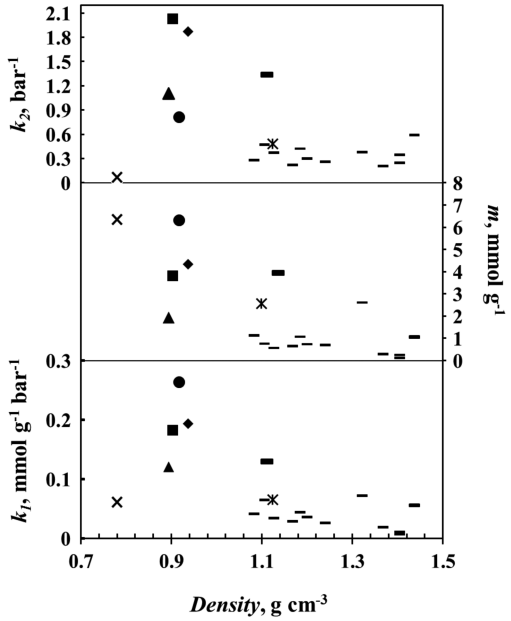

Figure 9. DM model constants for (■) Trip-TB ladder, (◆) Trip-TB network, (thick −) TB-cat-A, (▲) Indan-TB, (●) Trip(H)-PIM calculated from experimental data at 293 K. For comparison DM constants of (*) PIM-1,[74] (×) PTMSP[59] and (−) other glassy polymers[60−69] reported in Table 5 are shown.

Generally, the affinity and micropore capacity of PIMs are higher than those for other glassy polymers. The Langmuir saturation capacity constant (m), can be related to polymer structure; that is, PIMs as discussed previously cannot pack efficiently due to chains being contorted and rigid, unlike the usual glassy polymers (polycarbonates, polystyrenes, polyimides, etc.). Therefore, they possess much higher unrelaxed free volume and in turn can accommodate larger amounts of CO_2. It is worth noticing that PTMSP has a large Langmuirian capacity, similar to the PIMs with the highest micropore volume, but its overall solubility is similar to the other glassy polymers.

Tröger's base PIMs have the highest Langmuirian affinity for CO_2 among the glassy polymers, which is reflected in high k_2 values. The k_2 values of Trip-TB ladder and Trip-TB network are significantly higher than that of other polymers. It is likely that not only concentration of nitrogens but also pore shape contributes to the strength of CO_2 adsorption. The specific combination of Tröger's base and triptycene apparently have a synergetic effect because TB-cat-A and Indan-TB, which do not contain a triptycene unit, exhibit lower k_2 values compared to that of the triptycene TB PIMs. This is similar to properties reported for TB-EA-PIM.[25]

Triptycene-based PIMs have slightly higher Henry's law constants (k_1); that is, they are more likely to swell in presence of CO_2. In principle, swelling is an undesirable phenomena that alters polymer structure during sorption processes and may reduce gas selectivity.

Comparison of experimental and simulated total solubility at infinite dilution are shown in Figure 10. Samples generated without solvent overestimated CO_2 solubility, and better agreement is found with the samples generated in the presence of solvent, with the only exception being TB-cat-A.

Experiments allowed us to determine that the main contributions to the solubility S_0 are the micropore capacity m and the Langmuir affinity k_2, when the low contribution of the Henry's law constant to S_0 (less than 10%) is considered. Simulations, on the other hand, provide a molecular-level explanation based on the polymer microstructure.

The structural and thermodynamic properties of our models are summarized in Tables 6 and 7. In the case of models generated without solvent, polymers that do not contain triptycene units show the lowest value of S_0 (Indan-TB and TB-cat-A) and polymers containing triptycene have a slightly higher solubility. Solubility is inversely related to the average pore size, where more compact pores lead to a higher value of S_0. The models matching the experimental density, as mentioned above, show a better agreement in solubility, as expected for TB-cat-A. In general the solubility is higher in materials prepared without solvent and decreases with increasing the surface area (Figure 11). The differences in ASA for TB-cat-A generated with and without solvent molecules is not significant (Tables 6 and 7); within the error, the two surface areas are equivalent; hence, no differences in solubility values are observed between the two models.

Enthalpy of Adsorption. The enthalpy of adsorption of CO_2 is one of the critical parameters for consideration when evaluating an adsorbent for gas capture. The magnitude of the enthalpy of adsorption indicates the affinity of the adsorbent

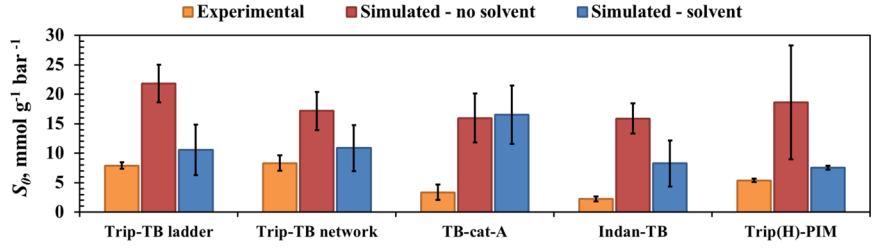

Figure 10. Comparison between experimental and simulated total solubility at infinite dilution.

dx.doi.org/10.1021/ie402846a | *Ind. Eng. Chem. Res.* 2013, 52, 16939−16950

Table 6. Geometric and Thermodynamic Properties of Polymer Models Generated without Solvents

polymer	$-\Delta H$, kJ mol^{-1}	S_0, mmol g^{-1} bar^{-1}	ASA, m^2 g^{-1}	total free volume, cm^3 g^{-1}	accessible free volume, cm^3 g^{-1}	$\langle\Phi\rangle$, Å
Trip-TB ladder	30.2(0.5)	21.8(3.2)	107(20)	0.082(4)	0.015(2)	1.4(4)
Trip-TB network	35.6(0.8)	17.2(4.1)	96(68)	0.080(6)	0.021(3)	2.2(1.9)
TB-cat-A	27.5(1.5)	15.9(3.3)	199(46)	0.097(4)	0.026(3)	1.3(5)
Indan-TB	26.4(0.4)	15.9(2.5)	117(18)	0.086(4)	0.014(2)	1.2(4)
Trip(H)-PIM	27.2(1.9)	18.6(9.4)	274(12)	0.103(6)	0.047(5)	1.7(3)

Table 7. Geometric and Thermodynamic Properties of Polymer Models Generated with Solvents

polymer	$-\Delta H$, kJ mol^{-1}	S_0, mmol g^{-1} bar^{-1}	ASA, m^2 g^{-1}	total free volume, cm^3 g^{-1}	accessible free volume, cm^3 g^{-1}	$\langle\Phi\rangle$, Å
Trip-TB ladder-S	26.0(0.5)	10.5(3.5)	975(31)	0.237(24)	0.159(21)	1.6(3)
Trip-TB network-S	27.8(1.0)	10.9(4.5)	918(67)	0.241(26)	0.164(24)	1.8(4)
TB-cat-A-S	26.1(0.7)	16.5(4.2)	350(99)	0.184(12)	0.100(10)	2.9(1.1)
Indan-TB-S	23.1(0.4)	8.3(3.7)	683(62)	0.187(20)	0.101(18)	1.5(4)
Trip(H)-PIM-S	27.6(0.6)	7.5(0.3)	1020(0)	0.310(0)	0.229(0)	2.2(0)

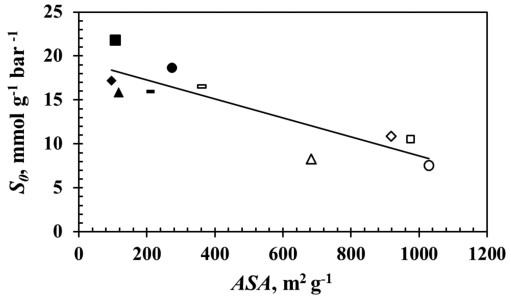

Figure 11. Simulated solubilities versus surface area for (■) Trip-TB ladder, (◆) Trip-TB network, (thick −) TB-cat-A, (▲) Indan-TB, and (●) Trip(H)-PIM. Solubilities calculated for models generated without solvent are represented by full symbols, and open symbols represent the models generated with the addition of solvent.

surface toward CO_2, which in turn allows determining the selectivity and the energy required to release the CO_2 molecules during regeneration.

Figure 12 shows the experimental enthalpy of adsorption at low coverage (ΔH) for different PIMs. Enthalpies of adsorption at high coverage are included in the Supporting Information.

The zero-coverage ΔH indicates the strength of the strongest binding sites within the adsorbent, which can be attributed to certain chemical features of the surface, in this case, the presence of basic nitrogen, or particular pore size and shape.

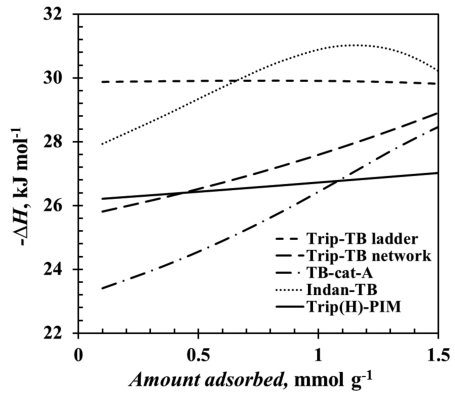

Figure 12. Experimental enthalpy of adsorption of CO_2 on the different polymers studied.

The ΔH at zero-coverage shown in Figure 12 follows the order TB-cat-A (23.2 kJ mol^{-1}) < Trip-TB network (25.6 kJ mol^{-1}) < Trip(H)-PIM (26.2 kJ mol^{-1}) < Indan-TB (27.6 kJ mol^{-1}) < Trip-TB ladder (29.9 kJ mol^{-1}).

The experimental trend in zero-coverage ΔH closely follows the trend in the average pore size reported in Tables 6 and 7 for model polymers that match the experimental density. Simulated ΔH values are remarkably similar to experimental ones (Figure 13). It is interesting that the composition of the polymer does not have a significant influence in the zero-coverage ΔH, even when it seems to be important for the solubility at zero-coverage. The small increase in $-\Delta H$ with the amount adsorbed can be explained by favorable later interactions between adsorbed molecules. Significant differences in the zero-coverage enthalpies of adsorption obtained for polymer structures generated with and without solvent are only observed for Trip-TB network. Minor differences are observed for the other materials. It should be noted that TB network structures without solvent were the least reproducible, evidenced by the larger error in ASA, which could explain the unusual behavior. Trip-TB network is the only material where the average pore size is smaller in the structures generated with solvent compared to those generated without solvent (Table 6 and Table 7).

■ CONCLUSIONS

Sorption of CO_2 on a selected number of microporous PIMs was studied at 273 and 333 K and over the pressure range of 0−20 bar to understand how their microstructure affects their potential in CO_2 capture. Sorption isotherms were described well by the dual mode sorption model, which allows comparing the performances of the polymers studied with those available in literature and significant differences were observed between PIMs and other glassy polymers.

This work has shown that tailoring PIMs has significant potential for improving membranes for gas separation, as higher solubilities and micropore void volumes can be obtained with a careful selection of the monomer structure and chemistry.

Madkour and Mark[71] have shown that modifications to the PIM structure from the chemistry of specific atoms in the monomer to the addition of side chains often results in a reduction in surface area that leads to a smaller permeability. Similarly, Larsen et al.[72] have shown that small modifications to the monomer chemistry can result in a marginal increase in capacity. Based on the results obtained in this work, the

dx.doi.org/10.1021/ie402846a | Ind. Eng. Chem. Res. 2013, 52, 16939−16950

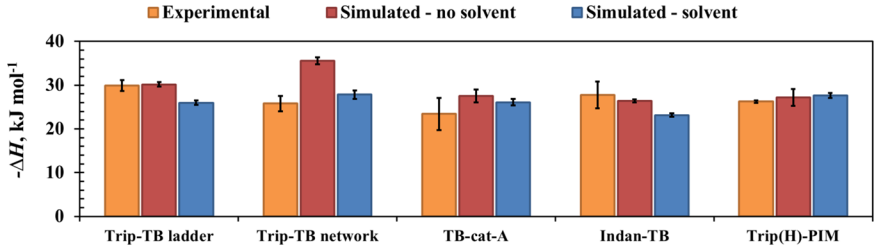

Figure 13. Comparison between experimental and simulated enthalpy of adsorption at low coverage.

following recommendations can be made for tailoring microporous polymers for CO_2 capture:

(I) The structure of the polymers should be designed to enhance the micropore volume and the Langmuirian affinity because they are the main contributors for the solubility (more than 90%).

(II) A high micropore volume can be achieved with triptycene-type contortion sites that generate sufficiently large voids. The accessible micropore volume and surface area are not necessarily related to the polymer density; therefore, care must be taken in selecting the monomer to avoid those that will generate a large volume of inaccessible pores. Even though Madkour and Mark[71] found that removing the contortion site reduced the accessible surface area by less than 10%, we found that Indan-TB has an accessible volume 40% smaller than TB-Cat-A, which suggests that the presence of a contortion site is crucial for these materials.

(III) Inclusion of TB groups that favorably interact with the CO_2 molecules enhances the Langmuirian affinity (k_2), even though evidence of specific interactions are not observed in the enthalpies of adsorption. Very large values of k_2 may not be beneficial because strong adsorption may reduce mobility. Madkour and Mark[71] showed that permeability in some gases is proportional to the accessible surface area, but in the case of CO_2, the key parameter is the solubility, highlighting the importance of the strength of the solid−fluid interaction in the membrane performance. They also found that modifying the chemistry of PIMs does not increase permeability, but their work focused exclusively on geometric considerations. Larsen et al.[72] have shown that introducing ketone groups as well as aromatic nitrogen groups marginally changes the adsorption isotherm, and Hart et al.[73] have shown that inserting sulfur containing groups may have a more significant effect in the isotherms.

(IV) The magnitude of Henry's solubility is not related to specific chemical interactions but gives an indication of the material's ability to swell. Network polymers have a higher Henrys's solubility, suggesting a higher ability to swell than linear or flexible polymers. Although swelling is undesirable, careful assessment of the impact of swelling on selectivity and permeability is needed before ruling out a potential polymer for future use.

(V) Simulations with and without solvent molecules also provide an indication of the material's potential to age. Aging can result in a reduction of pore size as well as in a reduction of ASA.

(VI) Zero-coverage enthalpies of adsorption are related to the pore size and the chemistry of the surface, making it difficult to modify by simply changing the monomer chemistry.

The discussion in this paper has focused on the behavior of the polymers in the presence of a single gas component (carbon dioxide), because the initial criteria for selecting a material should be related to the pure component properties. It should be remembered that for practical applications, gas selectivity plays a key role in defining the success of the process and that for the final selection of a material, knowledge of the behavior of mixtures, and the potential nonideal behavior of mixtures should also be considered. Given the large effort that is necessary for measuring properties of mixtures, the results presented from pure component measurements should encourage future research into properties of mixtures.

■ ASSOCIATED CONTENT

Supporting Information

Description of the computational method, the simulation box composition and volume, a complete list of the dual mode (DM) constants and enthalpy of sorption at high coverage. This information is available free of charge via the Internet at http://pubs.acs.org/.

■ AUTHOR INFORMATION

Corresponding Author

*F. R. Siperstein. E-mail: flor.siperstein@manchester.ac.uk.

Author Contributions

¶These authors contributed equally to the paper.

Notes

The authors declare no competing financial interest.

■ ACKNOWLEDGMENTS

The authors thank the Engineering and Physical Sciences Research Council (grant EP/G065144/1, EP/G062129/1, EP/G01244X, and EP/G062129/1) and the European Community's Seventh Framework Programme (FP7/2007-2013) project Double-NanoMem NMP3-SL-2009-228621 for funding. A.G. is grateful for the Postgraduate Studentship from The School of Chemical Engineering and Analytical Science of the University of Manchester. We are thankful to Professor Zeki Aktaş from the University of Ankara for collecting the BET surface area of Trip(H)-PIM and TB-cat-A samples during his visit to the University of Manchester.

■ REFERENCES

(1) Powell, C. E.; Qiao, G. G. Polymeric CO_2/N_2 gas separation membranes for the capture of carbon dioxide from power plant flue gases. *J. Membr. Sci.* **2006**, *279*, 1−49.

(2) MacLean, D. L.; Bollinger, W. A.; King, D. E.; Narayan, R. S. Gas Separations Using Composite Hollow Fiber Membranes. In *Recent*

Developments in Separation Science; Li, N. N., Calo, J. M., Eds.; CRC Press: Boca Raton, FL, 1986.
(3) Henis, J. M. S. Commercial and Practical Aspects of Gas Separation Membranes. In *Polymeric Gas Separation Membranes*; Paul, D. R., Yampol'skii, Y. P., Eds.; CRC Press: Boca Raton, FL, 1994.
(4) Backhouse, I. In *Effective Industrial Membrane Processes: Benefits and Opportunities*; Turner, M., Ed.; Springer: The Netherlands, 1991; pp 383−389.
(5) Sanders, E.; Clark, D. O.; Jensvold, J. A.; Beck, H. N.; Lipscomb, G. G.; Coan, F. L. Process for preparing POWADIR membranes from Tetrahalobisphenol A polycarbonate. U. S. Patent 4,772,392 1988.
(6) Baker, R. W. Future Directions on Membrane Gas Separation Technology. *Ind. Eng. Chem. Res.* **2002**, *41*, 1393−1411.
(7) Baker, R. W.; Lokhandwala, K. Natural Gas Processing with Membranes: An Overview. *Ind. Eng. Chem. Res.* **2008**, *47*, 2109−2121.
(8) Dong, X.; Jin, W.; Xu, N.; Li, K. Dense ceramic catalytic membranes and membrane reactors for energy and environmental applications. *Chem. Commun.* **2011**, *47*, 10886−10902.
(9) Chung, T.-S.; Jiang, L. Y.; Li, Y.; Kulprathipanja, S. Mixed matrix membranes (MMMs) comprising organic polymers with dispersed inorganic fillers for gas separation. *Prog. Polym. Sci.* **2007**, *32*, 483−507.
(10) Masuda, T.; Isobe, E.; Higashimura, T.; Takada, K. Poly[1-(trimethylsilyl)-1-propyne]: a new high polymer synthesized with transition-metal catalysts and characterized by extremely high gas permeability. *J. Am. Chem. Soc.* **1983**, *105*, 7473−7474.
(11) Budd, P. M.; Ghanem, B. S.; Makhseed, S.; McKeown, N. B.; Msayib, K. J.; Tattershall, C. E. Polymers of intrinsic microporosity (PIMs): robust, solution-processable, organic nanoporous materials. *Chem. Commun.* **2004**, 230−231.
(12) Ghanem, B. S.; Msayib, K. J.; McKeown, N. B.; Harris, K. D. M.; Pan, Z.; Budd, P. M.; Butler, A.; Selbie, J.; Book, D.; Walton, A. A triptycene-based polymer of intrinsic microposity that displays enhanced surface area and hydrogen adsorption. *Chem. Commun.* **2007**, 67−69.
(13) Ghanem, B. S.; McKeown, N. B.; Budd, P. M.; Fritsch, D. Polymers of Intrinsic Microporosity Derived from Bis(phenazyl) Monomers. *Macromolecules* **2008**, *41*, 1640−1646.
(14) Ghanem, B. S.; McKeown, N. B.; Budd, P. M.; Al-Harbi, N. M.; Fritsch, D.; Heinrich, K.; Starannikova, L.; Tokarev, A.; Yampolskii, Y. Synthesis, Characterization and Gas Permeation Properties of a Novel Group of Polymers with Intrinsic Microporsity: PIM-Polyimides. *Macromolecules* **2009**, *42*, 7881−7888.
(15) McKeown, N. B.; Budd, P. M. Exploitation of Intrinsic Microporosity in Polymer-Based Materials. *Macromolecules* **2010**, *43*, 5163−5176.
(16) Weber, J.; Su, Q.; Antonietti, M.; Thomas, A. Macromol. Rapid Commun. 18−19/2007. *Macromol. Rapid Commun.* **2007**, *28*, 1871−1876.
(17) Rose, M.; Bohlmann, W.; Sabo, M.; Kaskel, S. Element-organic frameworks with high permanent porosity. *Chem. Commun.* **2008**, 2462−2464.
(18) Stöckel, E.; Wu, X.; Trewin, A.; Wood, C. D.; Clowes, R.; Campbell, N. L.; Jones, J. T.; Khimyak, Y. Z.; Adams, D. J.; Cooper, A. I. High surface area amorphous microporous poly(aryleneethynylene) networks using tetrahedral carbon- and silicon-centred monomers. *Chem. Commun.* **2009**, 212−214.
(19) Schmidt, J.; Werner, M.; Thomas, A. Conjugated Microporous Polymer Networks via Yamamoto Polymerization. *Macromolecules* **2009**, *42*, 4426−4429.
(20) McKeown, N. B. Polymers of Intrinsic Microporosity. *ISRN Mater. Sci.* **2012**, *513986*, 16.
(21) Budd, P. M.; Msayib, K. J.; Tattershall, C. E.; Ghanem, B. S.; Reynolds, K. J.; McKeown, N. B.; Fritsch, D. Gas separation membranes from polymers of intrinsic microporosity. *J. Membr. Sci.* **2005**, *251*, 263−269.
(22) Robeson, L. M. Correlation of separation factor versus permeability for polymeric membranes. *J. Membr. Sci.* **1991**, *62*, 165−185.
(23) Robeson, L. M. The upper bound revisited. *J. Membr. Sci.* **2008**, *320*, 390−400.
(24) Freeman, B. D. Basis of Permeability/Selectivity Tradeoff Relations in Polymeric Gas Separation Membranes. *Macromolecules* **1999**, *32*, 375−380.
(25) Carta, M.; Malpass-Evans, R.; Croad, M.; Rogan, Y.; Jansen, J. C.; Bernardo, P.; Bazzarelli, F.; McKeown, N. B. An efficient polymer molecular sieve for membrane gas separations. *Science* **2013**, *339*, 303−307.
(26) Ghanem, B. S.; Hashem, M.; Harris, K. D. M.; Msayib, K. J.; Xu, M.; Budd, P. M.; Chaukura, N.; Book, D.; Tedds, S.; Walton, A.; McKeown, N. B. Triptycene-Based Polymers of Intrinsic Microporosity: Organic Materials That Can Be Tailored for Gas Adsorption. *Macromolecules* **2010**, *43*, 5287−5294.
(27) McKeown, N. B.; Carta, M.; Croad, M. U. K. Patent Appl. PCT/GB2011/051703; WO Patent 2012/035327 2010.
(28) Zhu, X.; Do-Thanh, C.-L.; Murdock, C. R.; Nelson, K. M.; Tian, C.; Brown, S.; Mahurin, S. M.; Jenkins, D. M.; Hu, J.; Zhao, B.; Liu, H.; Dai, S. Efficient CO_2 Capture by a 3D Porous Polymer Derived from Tröger's Base. *ACS Macro Letters* **2013**, *2*, 660−663.
(29) Meares, P. The Diffusion of Gases Through Polyvinyl Acetate. *J. Am. Chem. Soc.* **1954**, *76*, 3415−3422.
(30) Barrer, R. M.; Barrie, J. A.; Slater, J. Sorption and diffusion in ethyl cellulose. Part I. History-dependence of sorption isotherms and permeation rates. *J. Polym. Sci.* **1958**, *27*, 177−197.
(31) Michaels, A. S.; Vieth, W. R.; Barrie, J. A. Diffusion of Gases in Polyethylene Terephthalate. *J. Appl. Phys.* **2004**, *34*, 1−12.
(32) Vieth, W.; Sladek, K. A model for diffusion in a glassy polymer. *J. Colloid Sci.* **1965**, *20*, 1014−1033.
(33) Boquet, R.; Chirife, J.; Iglesias, H. A. Equations for fitting water sorption isotherms of foods. *Int. J. Food Sci. Technol.* **1978**, *13*, 319−327.
(34) Heuchel, M.; Fritsch, D.; Budd, P. M.; McKeown, N. B.; Hofmann, D. Atomistic packing model and free volume distribution of a polymer with intrinsic microporosity (PIM-1). *J. Membr. Sci.* **2008**, *318*, 84−99.
(35) Larsen, G. S.; Lin, P.; Hart, K. E.; Colina, C. M. Molecular Simulations of PIM-1-like Polymers of Intrinsic Microporosity. *Macromolecules* **2011**, *44*, 6944−6951.
(36) Fang, W.; Zhang, L.; Jiang, J. *J. Phys. Chem. C* **2011**, *115*, 14123−14130.
(37) Patel, H. A.; Je, S. H.; Park, J.; Chen, D. P.; Jung, Y.; Yavuz, C. T.; Coskun, A. Unprecedented high-temperature CO_2 selectivity in N_2-phobic nanoporous covalent organic polymers. *Nat. Commun.* **2013**, *4*, 1357.
(38) Zhao, L.; Zhai, D.; Liu, B.; Liu, Z.; Xu, C.; Wei, W.; Chen, Y.; Gao, J. Grand Canonical Monte Carlo simulations for energy gases on PIM-1 polymer and silicalite-1. *Chem. Eng. Sci.* **2012**, *68*, 101−107.
(39) Rappe, A. K.; Casewit, C. J.; Colwell, K. S.; Goddard, W. A.; Skiff, W. M. UFF, a full periodic table force field for molecular mechanics and molecular dynamics simulations. *J. Am. Chem. Soc.* **1992**, *114*, 10024−10035.
(40) Jorgensen, W. L.; Maxwell, D. S.; Tirado-Rives, J. Development and Testing of the OPLS All-Atom Force Field on Conformational Energetics and Properties of Organic Liquids. *J. Am. Chem. Soc.* **1996**, *118*, 11225−11236.
(41) Rappe, A. K.; Goddard, W. A. Charge equilibration for molecular dynamics simulations. *J. Phys. Chem.* **1991**, *95*, 3358−3363.
(42) Schaftenaar, G.; Noordik, J. Molden: a pre- and post-processing program for molecular and electronic structures. *J. Comput.-Aided Mol. Des.* **2000**, *14*, 123−134.
(43) Harms, S.; Rätzke, K.; Faupel, F.; Chaukura, N.; Budd, P. M.; Egger, W.; Ravelli, L. Aging and free volume in a polymer of intrinsic microporosity (PIM-1). *J. Adhes.* **2012**, *88*, 608−619.
(44) Sarkisov, L.; Harrison, A. Computational structure characterisation tools in application to ordered and disordered porous materials. *Mol. Simul.* **2011**, *37*, 1248−1257.

(45) Gelb, L. D.; Gubbins, K. E. Characterization of Porous Glasses: Simulation Models, Adsorption Isotherms, and the BET Analysis Method. *Langmuir* **1998**, *14*, 2097−2111.
(46) Walton, K. S.; Snurr, R. Q. Applicability of the BET method for determining surface areas of microporous metal-organic frameworks. *J. Am. Chem. Soc.* **2007**, *129*, 8552−8556.
(47) Bae, Y.; Yazaydin, A. O.; Snurr, R. Q. Evaluation of the BET Method for Determining Surface Areas of MOFs and Zeolites that Contain Ultra-Micropores. *Langmuir* **2010**, *26*, 5475−5483.
(48) Hart, K. E.; Abbott, L. J.; Colina, C. M. Analysis of Force Fields and BET Theory for Polymers of Intrinsic Microporosity. *Mol. Simul.* **2013**, *39*, 397−404.
(49) Accelrys Software Inc. *Materials Studio*, Release 5.5; Accelrys Software Inc.: San Diego, 2007.
(50) Mayo, S. L.; Olafson, B. D.; Goddard, W. A. DREIDING:A Generic Force Field for Molecular Simulations. *J. Phys. Chem.* **1990**, *94*, 8897−8909.
(51) Abbott, L. J.; Colina, C. M. Atomistic Structure Generation and Gas Adsorption Simulations of Microporous Polymer Networks. *Macromolecules* **2011**, *44*, 4511−4519.
(52) Abbott, L. J.; McDermott, A. G.; Del Regno, A.; Taylor, R. G. D.; Bezzu, C. G.; Msayib, K. J.; McKeown, N. B.; Siperstein, F. R.; Runt, J.; Colina, C. M. Characterizing the Structure of Organic Molecules of Intrinsic Microporosity by Molecular Simulations and X-ray Scattering. *J. Phys. Chem. B* **2013**, *117*, 355−364.
(53) Del Regno, A.; Taylor, R. G. D.; McKeown, N. B.; Siperstein, F. R. Organic molecules of intrinsic microporosity: Characterization of novel microporous materials. *Microporous Mesoporous Mater.* **2013**, *176*, 55−63.
(54) Robeson, L.; Burgoyne, W.; Langsam, M.; Savoca, A.; Tien, C. High performance polymers for membrane separation. *Polymer* **1994**, *35*, 4970−4978.
(55) Nagai, K.; Nakagawa, T. Effects of aging on the gas permeability and solubility in poly(1-trimethylsilyl-1-propyne) membranes synthesized with various catalysts. *J. Membr. Sci.* **1995**, *105*, 261−272.
(56) Morliére, N.; Valliéres, C.; Perrin, L.; Roizard, D. Impact of thermal ageing on sorption and diffusion properties of PTMSP. *J. Membr. Sci.* **2006**, *270*, 123−131.
(57) Merkel, T. C.; Freeman, B. D.; Spontak, R. J.; He, Z.; Pinnau, I.; Meakin, P.; Hill, A. J. Sorption, Transport, and Structural Evidence for Enhanced Free Volume in Poly(4-methyl-2-pentyne)/Fumed Silica Nanocomposite Membranes. *Chem. Mater.* **2003**, *15*, 109−123.
(58) Nagai, K.; Freeman, B. D.; Hill, A. J. Effect of physical aging of poly(1-trimethylsilyl-1-propyne) films synthesized with $TaCl_5$ and $NbCl_5$ on gas permeability, fractional free volume, and positron annihilation lifetime spectroscopy parameters. *J. Polym. Sci., Polym. Phys. Ed. Ed.* **2000**, *38*, 1222−1239.
(59) Srinivasan, R.; Auvil, S.; Burban, P. Elucidating the mechanism(s) of gas transport in poly[1-(trimethylsilyl)-1-propyne] (PTMSP) membranes. *J. Membr. Sci.* **1994**, *86*, 67−86.
(60) Kanehashi, S.; Nakagawa, T.; Nagai, K.; Duthie, X.; Kentish, S.; Stevens, G. Effects of carbon dioxide-induced plasticization on the gas transport properties of glassy polyimide membranes. *J. Membr. Sci.* **2007**, *298*, 147−155.
(61) Tanaka, K.; Kita, H.; Okamoto, K. Sorption of carbon dioxide in fluorinated poyimides. *J. Polym. Sci., Polym. Phys. Ed. Ed.* **1993**, *31*, 1127−1133.
(62) Aitken, C. L.; Koros, W. J.; Paul, D. R. Effect of structural symmetry on gas transport properties of polysulfones. *Macromolecules* **1992**, *25*, 3424−3434.
(63) Muruganandam, N.; Koros, W. J.; Paul, D. R. Gas sorption and transport in substituted polycarbonates. *J. Polym. Sci., Polym. Phys. Ed. Ed.* **1987**, *25*, 1999−2026.
(64) McHattie, J. S.; Koros, W. J.; Paul, D. R. Effect of isopropylidene replacement on gas transport properties of polycarbonates. *J. Polym. Sci., Polym. Phys. Ed. Ed.* **1991**, *29*, 731−746.
(65) Pixton, M.; Paul, D. Gas transport properties of polyarylates based on 9,9-bis(4-hydroxyphenyl)anthrone. *Polymer* **1995**, *36*, 2745−2751.
(66) Wright, C.; Paul, D. Gas sorption and transport in UV-irradiated polyarylate copolymers based on tetramethyl bisphenol-A and dihydroxybenzophenone. *J. Membr. Sci.* **1997**, *124*, 161−174.
(67) Puleo, A. C.; Muruganandam, N.; Paul, D. R. Gas sorption and transport in substituted polystyrenes. *J. Polym. Sci., Polym. Phys. Ed.* **1989**, *27*, 2385−2406.
(68) El-Hibri, M. J.; Paul, D. R. Effects of uniaxial drawing and heat-treatment on gas sorption and transport in PVC. *J. Appl. Polym. Sci.* **1985**, *30*, 3649−3678.
(69) Koros, W. J.; Paul, D. R. CO_2 sorption in poly(ethylene terephthalate) above and below the glass transition. *J. Polym. Sci., Polym. Phys. Ed.* **1978**, *16*, 1947−1963.
(70) Kanehashi, S.; Nagai, K. Analysis of dual-mode model parameters for gas sorption in glassy polymers. *J. Membr. Sci.* **2005**, *253*, 117−138.
(71) Madkour, T. M.; Mark, J. E. Molecular modeling investigation of the fundamental structural parameters of polymers of intrinsic microporosity for the design of tailor-made ultra-permeable and highly selective gas separation membranes. *J. Membr. Sci.* **2013**, *431*, 37−46.
(72) Larsen, G. S.; Lin, P.; Hart, K. E.; Colina, C. M. Molecular Simulations of PIM-1-like Polymers of Intrinsic Microporosity. *Macromolecules* **2011**, *44*, 6944−6951.
(73) Hart, K. E.; Abbott, L. J.; McKeown, N. B.; Colina, C. M. Toward Effective CO_2/CH_4 Separations by Sulfur-Containing PIMs via Predictive Molecular Simulations. *Macromolecules* **2013**, *46*, 5371−5380.
(74) Hölck, O.; Böhning, M.; Heuchel, M.; Siegert, M. R.; Hofmann, D. Gas sorption isotherms in swelling glassy polymers—Detailed atomistic simulations. *J. Membr. Sci.* **2013**, *428*, 523−532.